

Synthesis and application of montmorillonite nanocomposites/phenolic resins for the elimination of Basic Blue 41

Salima Lellou^a, Samir Kadi^{a,*}, Fatima Ouadjenia^b, Hadj Benhebal^c, Jacques Schott^d, Reda Marouf^b

^aLaboratoire de Physiologie Végétale Appliquée au Culture Hors Sol, Département des Sciences de la Nature et de la Vie, University of Tiaret BP 78 Zaaroura, Tiaret 14000, Algérie, emails: ksam792002@yahoo.fr (S. Kadi), lellousalima@yahoo.fr (S. Lellou)

^bLaboratory for Materials, Applications and Environment, University Mustapha Stambouli, Mascara, Algeria, emails: fouadjenia@gmail.com (F. Ouadjenia), r.marouf@univ-mascara.dz (R. Marouf)

^cDepartment of Chemistry, University of Tiaret BP 78 Zaaroura, Tiaret 14000, Algeria, email: benhebalh@yahoo.fr

^dLaboratoire Géosciences Environnement Toulouse (GET), CNRS-IRD-OMP-Université Toulouse, 14, Avenue Edouard Belin, 31400 Toulouse, France, email: jacques.schott@get.omp.eu

Received 28 June 2020; Accepted 19 December 2020

ABSTRACT

This work concerns the experimental study of the adsorption of Basic Blue 41 (BB41) by M'zila bentonite which has been modified by a polymer poly(p-hydroxybenzoic acid). These materials have been characterized by different techniques: X-ray diffraction, Fourier-transform infrared spectroscopy and scanning electron microscopy the analysis results confirm the structural in the basal distance from 15 Å to 12.80 Å. This suggests a partial exfoliation of the clay. The modified bentonite has a zero point of charge equal to 6.9. The raw and modified bentonite was used as an adsorbent for BB41. The optimum of these found parameters are a solid/solution ratio: 1 g L⁻¹, pH = 7 and equilibrium contact time 1 h. The kinetics of adsorption perfectly follows the pseudo-second-order model as well as that of intraparticle diffusion. The isotherms are of type S, they are well described by the Langmuir–Freundlich model ($R^2 > 0.96$). The adsorption of BB41 is spontaneous, exothermic and disordered for unmodified and modified bentonite.

Keywords: Bentonite; Polymer; Exfoliation; Adsorption; Basic Blue 41

1. Introduction

Preservation of our planet is one of the most occupying problems. Population growth and rapid industrialization are currently a serious threat to the survival of living organisms and endanger the ecological balance [1]. Nowadays, water pollution by dyes, pesticides and other organic pollutants causes serious problems for human health. These pollutants have the most toxic and dangerous effects [2,3]. Indeed, ~14 million chemicals exist in the environment

and are toxic beyond the threshold level [4]. Coloring compounds in addition to their toxicity, are resistant to biodegradation due to their recalcitrant behavior and their aromatic structures [5] and consequently, wastewater treatment has become a major environmental issue [6]. In order to cope with this situation, it has become vital to improving efficient and economical processes and techniques for water treatment [7]. Different depollution methods are developed for the removal of organic dyes [8], such as adsorption [9], biological methods and coagulation [10]. Adsorption

* Corresponding author.

is a suitable method due to its great potential for water disinfection [11]. Several works have been devoted to the use of clays as support for adsorbing organic or inorganic compounds [12–15]. Bentonite, as much as a clay mineral is a hydrous aluminum silicate, it's mainly made of silicon, aluminum and oxygen [16]. The main component of bentonite is montmorillonite which is a layered silicate material that belongs to the montmorillonite and smectite group of clay minerals [17,18]. In order to be used as well as adsorbents, clays have often been activated by acid or heat treatment. Research has also confirmed that the surface properties and reactivity of clay minerals can also be improved by intercalation of small organic species or polymers [19].

Montmorillonite is one of the most widely used clays in the synthesis of clay/polymer nanocomposites. In fact, it is very abundant and has very interesting properties such as its large specific surface area and excellent reactivity during modification. This gives it the possibility of intercalation and exfoliation by polymers in the interfoliar space [20]. Montmorillonite has several advantages for use as a support, including its lack of toxicity, chemical reactivity and hydrophilicity, allowing easy fixation of biomolecules [21–23].

Although phenolic resins are considered among the oldest synthetic polymers manufactured in commerce, their production and applications have continued to increase in various fields such as fireproofing, electronics and thermal insulation. Nevertheless, their properties are clearly superior when they are in the form of nanocomposites and especially with clays of the montmorillonite type [24].

The aim of this work is the valorization of the natural and abundant clay materials in Algeria into adsorbents with high adsorption capacity in order to eliminate water pollutants. Clay from the Mostaganem region in western Algeria has been modified by poly(p-hydroxybenzoic acid). The composite material obtained after its characterization by X-ray diffraction (XRD), Fourier-transform infrared spectroscopy (FTIR) and scanning electron microscopy (SEM), was used as a low-cost adsorbent carrier for the removal of Basic Blue 41 from an aqueous solution.

2. Materials and methods

2.1. Materials

In our study, we used local bentonite consisting essentially of montmorillonite. This clay comes from the deposits of M'zila, North-West of Algeria (Mostaganem). The latter is marketed without additives by BENTAL Company. Before use, the bentonite was purified. 20 g of clay is dispersed in 1 L of distilled water with magnetic stirring for 15 min at room temperature. After decanting for 24 h, the supernatant part is filtered and then dried at 80°C. For the removal of carbonates and organic matter, the clay was treated with HCl (0.1 N) and H₂O₂ (10 vol.), respectively. The clay is dried at 80°C and sieved to 80 µm.

p-hydroxybenzoic acid (99%), NH₄OH (30%), HCHO (37%), NaOH, and HCl (37%) were all of the analytical grade, obtained from Panreac (España) and Merck (Germany).

Basic Blue 41 (BB41) known as blue bezacryl 300 GR, is a cationic dye used in the textile industry whose formula is C₂₀H₂₆N₄O₆S₂. The structure of BB41 is reported in Fig. 1.

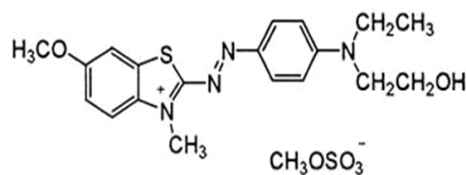


Fig. 1. Structure of Basic Blue 41.

2.2. Synthesis of nanocomposite

M'zila bentonite was modified by poly(p-hydroxybenzoic acid) (poly-PHABA), by *in-situ* polymerization. For this, 27.6 g of clay were introduced into a three-necked flask equipped with a condenser (reflux mounting) mixed with 0.1 mol p-hydroxybenzoic acid, 0.15 mol of 37% formaldehyde and 70 mL of distilled water. The mixture is heated at 90°C for 10 min. Using a separatory funnel, 7 mL of NH₄OH (34%) are added. The mixture is left under stirring for 3 h. After filtration, the filtrate is washed several times with cold water and then a second time with hot water to remove the excess of unreacted reagents. The complex is dried at 70°C for 24 h then crushed and sieved at 80 µm.

2.3. Characterization of the materials

The materials were characterized by XRD, FTIR, SEM and pH_{PZC}. X-ray powder diffraction patterns were obtained using a Bruker phaser 2 (USA) diffractometer with CuKα radiation operating at 40 kV and 25 mA. The XRD data were collected over a 2 h range of 5°–90° with a step width of 0.01°. The infrared spectra were acquired through a Fourier-transform infrared spectrometer. The device used is SHIMADZU FTIR-8400S (Japan). The structure band region (400–4,000 cm⁻¹) was investigated using KBr wafers containing 0.5% of the sample. The morphological analysis is performed by a JSM-7200F scanning electron microscope with a field-effect gun (Schottky, Germany).

The zero charge point was measured as follows: a 20 mL batch of 0.01 M KNO₃ solution was placed in closed Erlenmeyer flasks. The pH was adjusted by adding 1 M HCl or 1 M NaOH solutions in the pH range of 2 to 10. Then, 0.1 g of the sample was added to each Erlenmeyer flask followed by stirring for 24 h under atmospheric conditions. When the final pH was determined, we plotted the ΔpH (final pH – initial pH) as a function of initial pH. The pH_{PZC} corresponds to the point of intersection of this plot with the x-axis [25].

2.4. Adsorption procedure

The adsorption experiments of Basic Blue 41 were performed via the batch method at 20°C ± 1°C. 0.02 g of the bentonite was mixed with 20 mL of BB41 in a concentration range of 10–200 mg L⁻¹. The experimental conditions are outlined in Table 1. The dispersions pH was adjusted by adding 0.1 M HCl or 0.1 M NaOH. After each experiment, the solution was separated by filtration. The filtrate was analyzed by visible spectrophotometry at λ = 600 nm using a Shimadzu-1240 UV-Vis spectrophotometer.

Table 1
Experimental conditions during the adsorption of Basic Blue 41

Adsorbent concentration	Clay: 1, 2, 3, 4, 5, 6, 7, 8, 9, and 10 g L ⁻¹ ; temperature: 20°C; contact time: 2 h
pH	pH (BB41): 2, 3, 4, 5, 6, 7, 8, 9, and 10; clay: 1 g L ⁻¹ ; temperature: 20°C; contact time: 2 h
Kinetics	Contact time: 1, 3, 5, 10, 20, 30, 60, 90, and 120 min; clay: 1 g L ⁻¹ ; temperature: 20°C; pH: 7
Isotherms	(BB41): 10, 20, 40, 60, 100, 150, and 200 mg L ⁻¹ ; clay: 1 g L ⁻¹ ; temperature: 20°C; contact time: 1 h; pH: 7
Temperature	Temperature: 20°C, 30°C, and 40°C; clay: 1 g L ⁻¹ ; (BB41): 10, 20, 40, 60, 100, 150, and 200 mg L ⁻¹ ; contact time: 1 h; pH: 7

The amounts of adsorbed BB41, (mg g⁻¹), were determined using the following equation:

$$Q_e = \frac{(C_0 - C_e)}{m} V \quad (1)$$

where C_0 and C_e are the initial and the equilibrium dye concentrations (mg L⁻¹), V is the volume of dye solution used (L), and m is the mass of material used (g).

2.5. Theoretical considerations

2.5.1. Adsorption kinetics

In order to study the mechanism that controls the adsorption process, various kinetic equations have been applied to model the adsorption kinetics of Basic Blue 41 by purified and modified clays. These models are grouped in Table 2.

2.5.2. Adsorption isotherms modeling

The equilibrium models of Langmuir, Langmuir [29], Freundlich [30], and Langmuir–Freundlich [31] were used to fit the experimental data. These models are grouped in Table 3.

2.5.3. Thermodynamic study

The thermodynamic parameters for the adsorption process ΔG° , ΔH° , and ΔS° , were evaluated using the equation:

$$\ln K_d = \left(-\frac{\Delta H^\circ}{RT} \right) + \left(\frac{\Delta S^\circ}{R} \right) \quad (2)$$

where ΔH° and ΔS° are the enthalpy (J mol⁻¹) and entropy change (J mol⁻¹ K⁻¹), respectively. T is the absolute temperature (K), R gas constant (J mol⁻¹ K⁻¹), and K_d is the distribution coefficient (L g⁻¹). This coefficient is given by:

$$K_d = \frac{Q_e}{C_e} \quad (3)$$

The enthalpy and entropy changes are determined graphically by plotting $\ln K_d$ vs. $1/T$, which gives a straight line. According to thermodynamics, the Gibbs free energy change, ΔG° , is related to ΔH° and ΔS° at constant temperature by the following equation:

$$\Delta G^\circ = \Delta H^\circ - T\Delta S^\circ \quad (4)$$

Table 2
Equations of the different kinetic models

Kinetic models	Equations
Pseudo-first-order model [23]	$\log(Q_e - Q_t) = \log Q_e - \frac{k_1 \cdot t}{2.303}$
Pseudo-second-order model [24]	$\frac{t}{Q_t} = \left(\frac{1}{K_2 \cdot Q_e^2} \right) + \frac{t}{Q_e}$
Intraparticle diffusion [25]	$Q_t = K_{id} \cdot t^{1/2} + C$

Table 3
Equations of the different adsorption isotherms

Isotherm model	Equation
Langmuir [26]	$\frac{C_e}{Q_e} = \frac{1}{Q_m K_L} + \frac{C_e}{Q_m}$
Freundlich [27]	$\log Q_e = \log K_F + \frac{1}{n} \log C_e$
Langmuir–Freundlich [28]	$Q_e = Q_m \frac{(K_{LF} C_e)^{1/n}}{1 + (K_{LF} C_e)^{1/n}}$

3. Results and discussion

3.1. XRD analysis

The mineralogical analysis of the purified and modified bentonite was carried out by XRD. The apparatus consists of a Bruker phaser 2 diffractometer, using CuK α radiation, wavelength $\lambda = 1.5406 \text{ \AA}$, operating at 40 kV and 25 mA. XRD data were collected over a 2θ range from 5° to 30°.

The diffractograms of the different samples are shown in Fig. 2. The XRD spectrum of the starting material, bentonite (B), shows a high intensity at $2\theta = 5.887^\circ$, which corresponds to the basal distance of the sheet from the plane (001) and which is equal to 15 Å. It is the characteristic peak of montmorillonite [32]. Other peaks linked to kaolinite are observed at 2θ equal to 12.33, 19.803 and 23.094° which correspond respectively to the network planes (011), (020) and (021). The peaks noted at 2θ equal to 20.827° and 26.594° are characteristic of quartz.

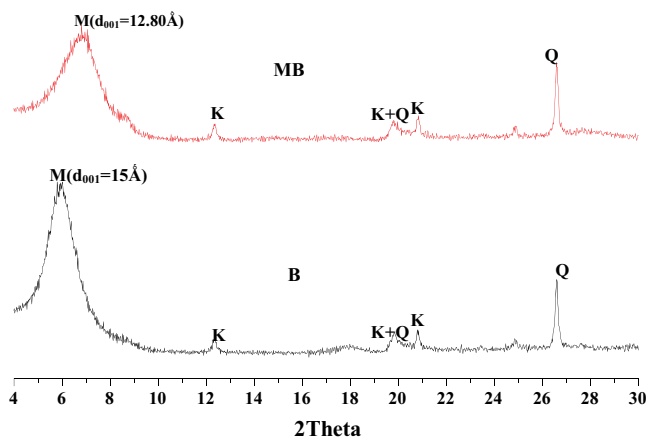


Fig. 2. XRD patterns of unmodified bentonite (B) and modified (MB).

For bentonite modified with poly(p-hydroxybenzoic acid), modified bentonite (MB), it can be noted that poly-PHABA caused considerable changes within montmorillonite. Indeed, there is a decrease in intensity, a widening of the characteristic peak and a decrease in its basal distance from 15 Å to 12.80 Å. This reveals a poorly organized structure and a progressive amorphization of the structure, probably due to the in situ polymerization of the interfoliar space of montmorillonite [33–35]. We can suggest a partial exfoliation of the clay.

3.2. FTIR analysis

The FTIR spectra of both samples are shown in Figs. 3 and 4. The spectrum of purified bentonite (B) shows two bands in the 3,700–3,600 cm^{-1} region. This region is particularly related to the stretching vibrations of the hydroxyl groups. The 3,688 cm^{-1} band is attributed to the –OH vibrations of the inner surface. The band at 3,636 cm^{-1} is due to the elongation vibration of the internal hydroxyls [36]. The interfoliar water is represented by the band at 3,550 cm^{-1} [37]. The 1,630 cm^{-1} band is assigned to adsorbed water [bend] deformation, while the 1,116 cm^{-1} band is due to the apical Si–O stretching mode. The bands between 1,000 and 400 cm^{-1} are attributed to Si–O–Si, Al–OH and OH vibrations. The bands observed at 2,899 and 2,337 cm^{-1} are due to the presence of calcite and quartz respectively [38].

The modified bentonite (MB) has new bands in the area of 1,165 at 1,685 cm^{-1} . They are attributed to the aromatic elongation vibrations of the C=C bond. The 1,278 cm^{-1} band is affiliated to the asymmetric stretching vibration of the C–C–O bond [39]. The band observed at 1,165 cm^{-1} is attributed to both the extensional vibrations of the C–O bond of the aromatic ring and the carboxylic acid. The 1,685 cm^{-1} band is due to the elongation vibrations of the C=O bond of the carboxylic acid. The 1,397 cm^{-1} band is allocated to C–OH vibrations. After the adsorption of BB41 by the purified and modified bentonite (Fig. 4), we notice the appearance of new bands. The bands observed at 2,983 and 2,897 cm^{-1} are attributed to the elongation vibrations of the C–H bond. The band noticed at 1,735 cm^{-1} is affected by the vibrations of elongation of the C=N bond of

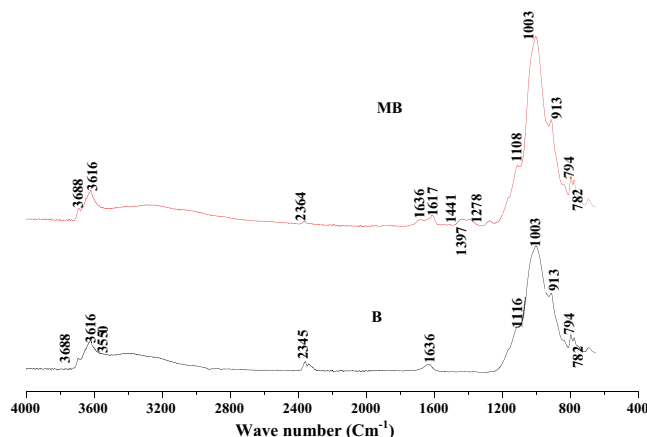


Fig. 3. FTIR spectra of unmodified and modified bentonite.

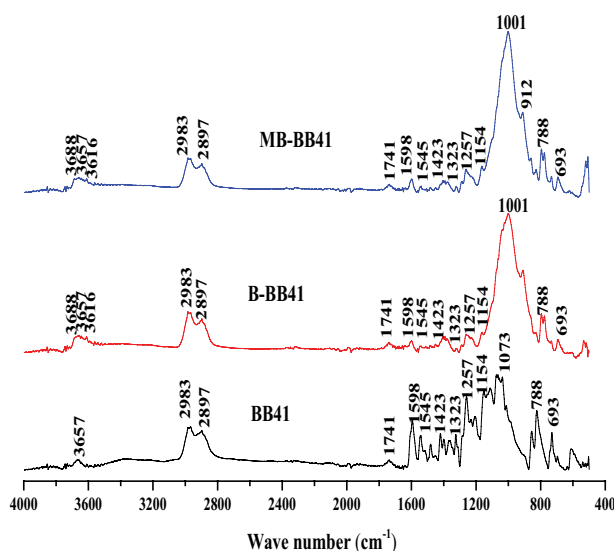


Fig. 4. FTIR spectra of unmodified and modified bentonite after adsorption of BB41.

the aromatic ring. The bands 1,598, 1,545 and 1,423 cm^{-1} are allocated to the vibrations of elongation of the C=C bond of the aromatic ring. The bands 1,257 and 1,323 are credited with the C–N bond elongation vibrations of the aromatic ring [40].

3.3. Scanning electron microscopy

The images made by the SEM of the two materials B and MB are shown in Fig. 5. Fig. 5a shows the presence of heterogeneous aggregates of different shapes and sizes. It appears that these grains constitute a stack of leaflets probably representing the clay layers.

Figs. 5b–d show a degree of disorder in the morphology of the clay. Dark platelets correspond to monolayers, also called silicate nanolayers. The silicate nanoplates are oriented in all directions, but they are not separated from each other which favors an exfoliated structure [41]. The silicate nanolayers are 55.62 nm in length, 33.75 in width and 65.06 in diameter. Figs. 5e and f show that

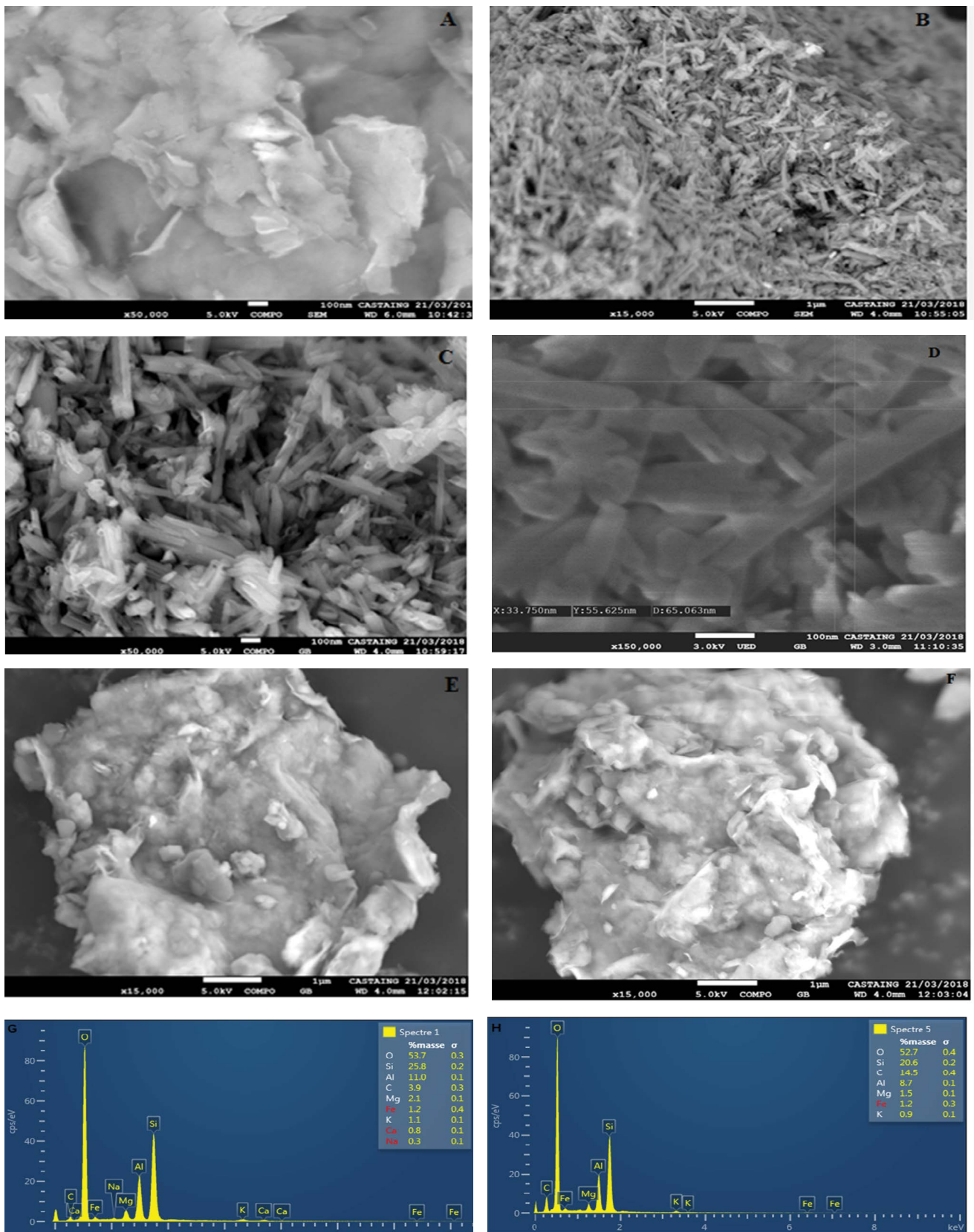


Fig. 5. Scanning electron microscopy and EDX images of unmodified (B) and modified bentonite (MB).

some of the clay has not been exfoliated, which is in line with XRD.

The energy-dispersive X-ray spectroscopy (EDX) results for unmodified and modified bentonite are shown in Figs. 5g and h respectively. As can be seen in these figures, the in situ polymerization of p-hydroxybenzoic acid caused a substantial change in the chemical composition of the clay. Indeed, the in situ polymerization caused a significant increase in the carbon content which went from 3.9% for the unmodified bentonite (B) to 14.5% for the modified bentonite. For the other constituents, their contents remain more or less stable.

3.4. Zero charge point

Fig. 6 shows the $pH_i - pH_f$ evolution as a function of pH_i . The point of intersection of the graph with the abscissa of X represents the point of zero charge (pH_{PZC}), in this point, the surface charge of the solid is then globally neutralized.

According to the graph, the bentonite (B), has a zero point of charge equal to 5. For the modified bentonite (MB), the isoelectric point is observed at $pH = 6.9$. This shows that the acidic poly(p-hydroxybenzoic acid) caused great changes in our clay.

At $pH < pH_{PZC}$ the surface of bentonite becomes positively charged. On the other hand at $pH > pH_{PZC}$ the surface of the clay will be negatively charged [42].

3.5. Adsorption of Basic Blue 41

3.5.1. Effect of adsorbent dose

The evolution of the amount of Basic Blue 41 adsorbed per unit mass of clay as a function of the solid/liquid ratio is shown in Fig. 7.

According to this figure, there is a decrease in the equilibrium adsorbed amount of Basic Blue 41 as the amount of adsorbent increases. This behavior can be explained by the fact that the presence of a large amount of adsorbent reduces the number of adsorption sites per unit mass, which causes a decrease in adsorption. On the other hand, increasing the amount of adsorbent will cause the

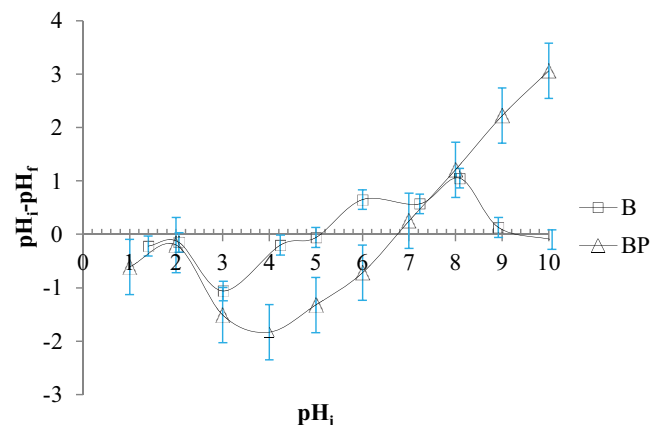


Fig. 6. Determination of pH_{PZC} point of unmodified (B) and modified bentonite (MB).

formation of aggregates; leading to a decrease in the total area and an increase in the length of the diffusion path. These two phenomena contribute to the decrease of the adsorbed quantity per unit of mass [43,44]. Thus, 1 g L^{-1} was considered in all subsequent experiments.

3.5.2. Effects of pH

The pH is one of the most influencing factors on adsorption because it affects not only the material charge but also the degree of ionization of the materials, the dissociation of the functional groups on the active sites of the adsorbent and the ionization of dye molecules in solution. In order to study the influence of pH on the retention of BB41 by purified and modified bentonite, we have taken a pH range of 2 to 10. Fig. 8 shows the evolution of the amount of dye adsorbed at equilibrium Q_e (mg g^{-1}) as a function of pH onto B and MB.

As shown in Fig. 8, the adsorption capacity of BB41 by B is not influenced by the rise in pH. For modified

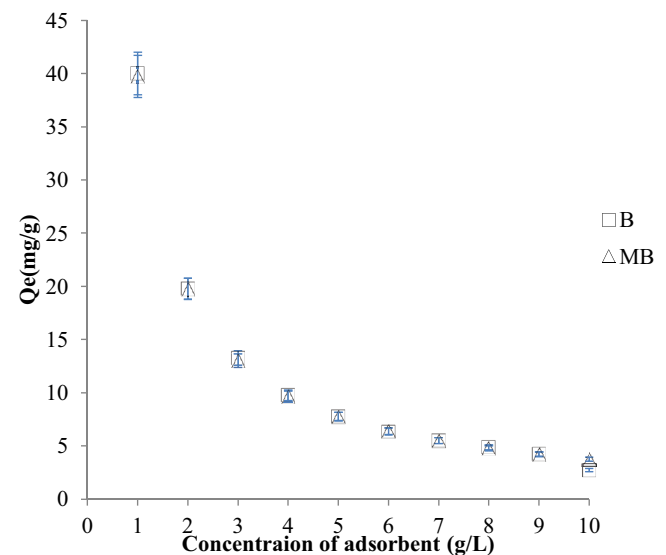


Fig. 7. Effect of solid/solution concentration on the amount adsorbed by the unmodified (B) and modified bentonite (MB).

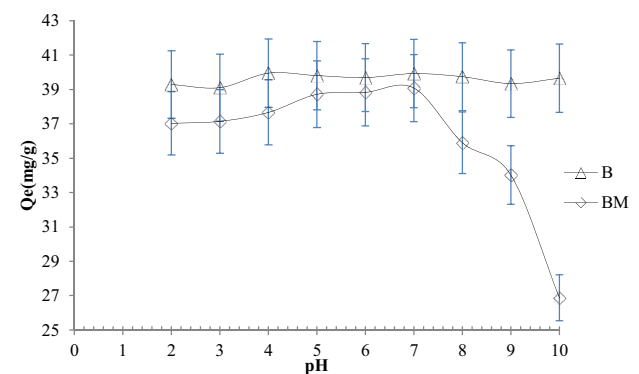


Fig. 8. Effect of pH on the adsorption of BB41 onto the bentonite solids.

bentonite, there is an increase in the amount of Basic Blue 41 adsorbed in the pH range from 2 to 7 and after that, it decreases. This can be explained by the fact that at pH less than 7, $pH < pH_{pZC}$, the modified bentonite is positively charged. Therefore, it has an electrostatic repulsion between the modified clay and the cationic groups of the dye. But in addition to that, it has a competitive effect between the H^+ ions and the cationic groups of the dye. The latter is more important than the electrostatic repulsion, which will explain the strong adsorption of this dye in this pH range [45,46]. At pH values above 7 ($pH > pH_{pZC}$), the surface of the modified bentonite is negatively charged. Normally there will be strong adsorption of this dye in this pH range. However, the opposite has happened. In this pH range, the molecules of the dye become neutral which will reduce the amount of adsorbed BB41 [47]. Similar pH behaviors have been observed upon adsorption of cationic dyes by different materials [48–50].

3.5.3. Effect of contact time

In order to study the effect of time on the adsorption of Basic Blue 41 by the two materials, a series of experiments were carried out at $pH = 7$ and for a dose of sorbent equal to 1 g L^{-1} in time intervals ranging from 1 to 120 min (Fig. 9). Depending on the path of the curve, an increase in

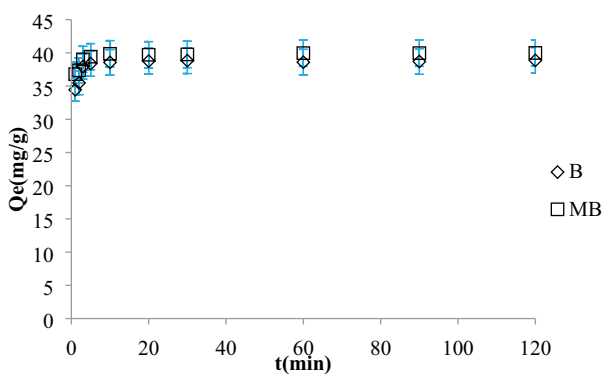


Fig. 9. Effect of contact time on the fixation of BB41 by B and MB.

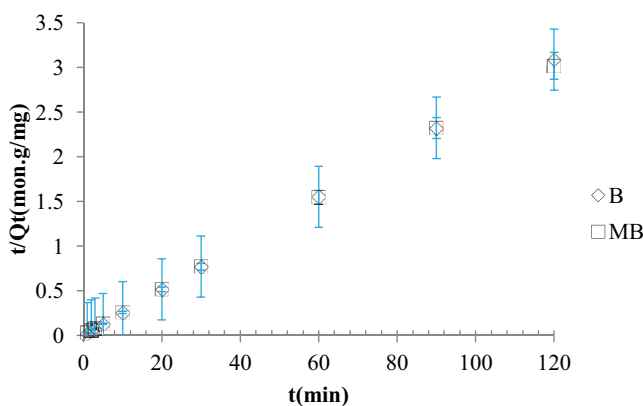


Fig. 10. Application of the pseudo-second-order model to BB41 adsorption by B and MB.

the adsorbed quantity of BB41 (40 mg L^{-1}) was observed in the first 10 min, then it stabilized. Equilibrium is reached after 60 min for the two samples. Similar results were found by Yazdanshenas et al. [51] during adsorption of BB41 by coconut fiber particles.

To describe the kinetics of adsorption of Basic Blue 41 by purified and modified bentonite, three kinetic models were used which are pseudo-first-order, pseudo-second-order and intraparticle diffusion. The parameters corresponding to the kinetic models used are reported in Table 4. The values of the regression coefficients are extremely low, $R^2 < 0.76$, for the first model. The adsorption of BB41 by two materials does not follow Lagergren’s equation of the first order (figure not shown). The results show that the adsorption of Basic Blue 41 perfectly follows the pseudo-second-order model for both materials (Fig. 10). The coefficients of determination, tend towards 1. The calculated values, $Q_{e,cal}$ also agree very well with the experimental data (Table 4). Given the initial adsorption rate h , with $h = K_2 \cdot Q_e^2$, the modified bentonite adsorbs BB41 faster than the starting material. The results of the intraparticle diffusion model are presented in Fig. 11 and in Table 4. The coefficients of determination of the second section are equal to unity, which confirms the contribution of this phenomenon in the kinetics of adsorption of BB41 by the two materials. The slope of the second section characterizes the rate constant of the intraparticle diffusion, K_{id} and the intercept, C , representing the thickness of the boundary layer.

The K_{id} and C values remain unchanged between B and MB, suggesting that intraparticle scattering is not the only factor responsible for the adsorption rate.

Pseudo-second-order and intraparticle diffusion models have been successfully applied in the adsorption of Basic Blue 41 by nanoporous silica [52].

3.6. Adsorption equilibrium

3.6.1. Isotherms

Using the classification of Giles et al. [53], the adsorption isotherms of Basic Blue 41 are type S (Fig. 12).

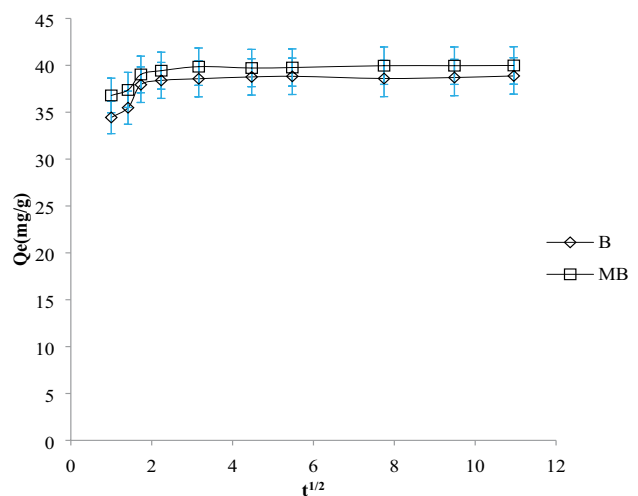


Fig. 11. Application of the intraparticle diffusion model to BB41 adsorption by B and MB.

Table 4
Kinetic parameters Basic Blue 41 adsorption onto the bentonite solids

Samples	Pseudo-first-order model			Pseudo-second-order model			Intraparticle diffusion model				
	$Q_{e,exp}$ (mg g ⁻¹)	K_1 (min ⁻¹)	$Q_{e,cal}$ (mg g ⁻¹)	R^2	$Q_{e,cal}$ (mg g ⁻¹)	K_2 (g mg ⁻¹ min ⁻¹)	h (mg g ⁻¹ min ^{-1/2})	R^2	K_{id} (mg g ⁻¹ min ^{-1/2})	C (mg g ⁻¹)	R^2
Unmodified bentonite	38.87	0.025	0.83	0.26	38.76	0.24	357.14	1	0.90	36.37	1
Modified bentonite	39.75	2.574	0.03	0.33	39.37	0.07	107.52	0.99	0.70	36.36	0.99

The S-type curves appear when the adsorption of the solvent is appreciable because the adsorption becomes progressively easier as the quantity adsorbed increases, this can be explained by the existence of a cooperative synergistic effect; the adsorbed molecules facilitate the adsorption of the following molecules, due to the adsorbate–adsorbate side attraction. This arrangement is favored when the solvent rivals the solute for occupying the adsorption sites.

The results revealed a decrease in adsorption capacity as the temperature rose from 20°C to 30°C, such that the amount adsorbed at equilibrium fell from 196 to 187 mg g⁻¹ for unmodified bentonite and from 198 to 186 mg g⁻¹ for the modified bentonite. On the other hand, when the temperature rose to 40°C, the amount adsorbed at equilibrium increased to reach 195 mg g⁻¹ for B and 196 mg g⁻¹ for MB.

The results show that the adsorption is exothermic in the temperature range of 20°C–30°C and then becomes endothermic. The increase in adsorption of BB41 at 40°C can be attributed to the increase in the number of active sites available or to the improvement in the mobility of BB41 molecules [54].

Similar behavior was observed during lead adsorption by a heat-treated Algerian halloysite. The adsorption was exothermic in the temperature range of 25°C–40°C and then became exothermic at 55°C [43]. The values of the maximum adsorption capacity of BB41 by the various adsorbents are shown in Table 5. The results show that MB has a great potential for adsorption of this cationic dye with an adsorption capacity, 198 mg g⁻¹, higher than other adsorbents.

3.6.2. Affinity of adsorption

The adsorption affinity is the amount of Basic Blue 41 adsorbed by the samples, at a given temperature, relative to the equilibrium concentration. This relative affinity to our different materials, measured at 20°C, is shown in Fig. 13.

We note that MB has the greatest affinity for the retention of Basic Blue 41. The greater adsorption capacity of BB41 is attributed to the nanocomposite (MB) with an equilibrium adsorbed amount of 197.37 mg g⁻¹.

3.6.3. Fitting the models to the experimental data

In order to describe our experimental isotherms, three models were used (Langmuir, Freundlich and Langmuir–Freundlich). The constants of these models are presented in Table 6. The results obtained revealed that the Langmuir model does not reflect our experimental isotherms. This model suggests that adsorption occurs at the surface with similar adsorption energies and that there is no interaction between the adsorbed molecules. The fit of the experimental data by the Freundlich model appears better compared to the Langmuir model with regression coefficients between 0.60 and 0.95. This model suggests that there are different types of adsorption sites with different energies, exponentially distributed according to the heat of adsorption. This distribution of interaction energies is explained by the heterogeneity of the sites. The adsorption capacity K_f increases with increasing temperature for both

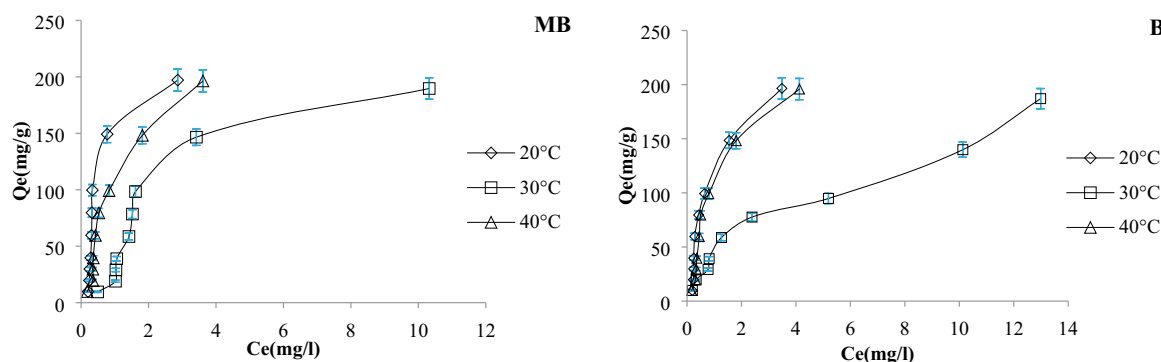


Fig. 12. Isotherms of adsorption of BB41 by unmodified (B) and modified bentonite (MB).

Table 5
Adsorption capacities of different adsorbent materials for BB41 dye removal

Adsorbant	Initial concentration (mg L ⁻¹)	Dosage (g L ⁻¹)	pH	Time	Q _{max} (mg g ⁻¹)	References
Spent waste biomass	150	0.006	7	14 h	24	[55]
Coconut shell activated carbon	16	0.5	6	1 h	62	[56]
Saudi local clay mineral	1,000	1	Natural	24 h	73	[57]
Activated carbon prepared from filamentous algae	100	1	9	90 min	125	[58]
N, F-codoped flower-like TiO ₂ microspheres	80	0.625	8	1 h	143	[59]
Modified bentonite by poly(p-hydroxybenzoic acid)	200	1	7	1 h	198	This work

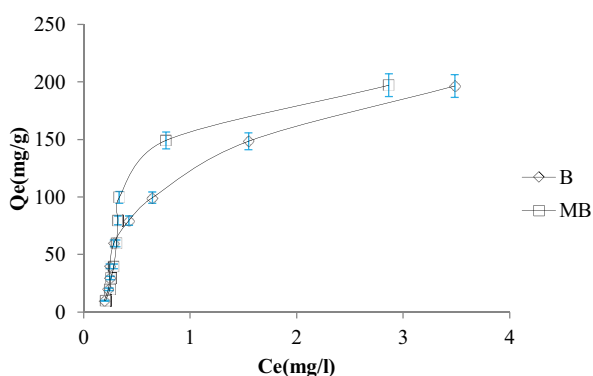


Fig. 13. Adsorption affinity of BB41 by unmodified (B) and modified bentonite (MB). Experimental conditions: $T = 20^{\circ}\text{C}$; $R = 1 \text{ g L}^{-1}$; $t = 60 \text{ min}$; $\text{pH} = 7$.

materials. The coefficient n varies with temperature; it characterizes the intensity of adsorption. Whatever the sample, $n > 1$ indicates a favorable adsorption process.

Adsorption is a very complex phenomenon because different interactions can be at the origin of the association of a chemical product (adsorbate) with a solid (adsorbent). Two-parameter models such as those of Langmuir and Freundlich cannot explain equilibrium relations very

well. For this reason, it is necessary to use the three-parameter model such as the Langmuir–Freundlich model to describe the experimental isotherms. From the values of the coefficient of determination, R^2 , we can affirm that the Langmuir–Freundlich equation describes very well the adsorption BB41 by the two materials. Whatever the temperature, $R^2 \geq 0.960$ and a low mean relative error, E (%), which does not exceed 35.65% (Table 6).

3.7. Thermodynamic parameters

The heats adsorption ΔH° , ΔS° and ΔG° are given in Table 7. In the case of physisorption, the variation of the enthalpy is between 0 and 20 kJ mol⁻¹, as for the chemisorption is in the range of 80–400 kJ mol⁻¹ [60]. The negative values of ΔG° imply the spontaneity of the physisorption process. However, the Gibbs energy increases with increasing temperature for both materials, indicating the increase of this spontaneous character.

The results obtained from the thermodynamic study indicate that the values of ΔH° are positive which means the BB41 adsorption is endothermic and physis in nature and an increase in temperature favors the process. The positive values of ΔS° suggest much more disordered adsorbate–adsorbent systems located at inter-face solid/liquid [61]. The molecules of the Basic Blue 41 are much more chaotic in the adsorbed state than in the solution [39,46].

Table 6
Isotherm parameters for the BB41 adsorption at different temperatures

Samples	T (°C)	Langmuir			Freundlich			Langmuir–Freundlich							
		$Q_{e,exp}$ (mg g ⁻¹)	Q_m (mg g ⁻¹)	K_L (L mg ⁻¹)	R^2	E (%)	K_F (L g ⁻¹)	n	R^2	E (%)	Q_{max} (mg g ⁻¹)	n	K_{LF} (L mg ⁻¹)	R^2	E (%)
Unmodified bentonite	20	196.52	434.78	0.28	0.22	38.60	92.35	1.46	0.75	48.36	204.95	0.650	1.830	0.96	35.65
	30	179.35	222.22	0.23	0.92	11.23	37.49	1.57	0.95	14.97	1,202.45	1.631	1.005	0.97	17.36
	40	194.88	434.78	0.23	0.36	28.36	84.81	1.11	0.83	38.24	204.89	0.617	1.318	0.99	20.80
Modified bentonite	20	209.43	555.55	0.22	0.068	48.09	121.77	1.09	0.60	61.30	173.59	0.139	2,783.28	0.96	13.68
	30	187.61	555.56	0.06	0.524	41.50	32.35	1.00	0.78	41.51	183.19	0.350	0.205	0.97	14.64
	40	143.06	625	0.149	0.136	30.79	76.73	1.18	0.66	50.26	209.86	0.617	1.199	0.97	24.17

Table 7

Thermodynamic parameters for adsorption of Basic Blue 41 by different materials

Samples	BB41				
	ΔH° (kJ mol ⁻¹)	ΔS° (kJ mol ⁻¹ K ⁻¹)	ΔG° (kJ mol ⁻¹)		
			20°C	30°C	40°C
Unmodified bentonite	7.707 ± 0.21	0.056 ± 0.67	-8.834	-9.111	-9.666
Modified bentonite	0.685 ± 0.02	0.033 ± 0.15	-9.184	-9.349	-9.680

4. Conclusion

M'zila bentonite has been modified by the poly(p-hydroxybenzoic acid). This modification caused considerable changes in the structure of the clay. Indeed, a decrease and widening of the characteristic peak of montmorillonite have been observed, leading to a decrease in the distance of the (001) montmorillonite planar planes from 15 Å to 12.80 Å. This suggests that there is partial exfoliation of the clay. These results were confirmed by the SEM. The unmodified and modified bentonite was used as adsorbent support for Basic Blue 41. The parameters considered after optimization are a solid/solution ratio: 1 g L⁻¹, pH = 7 and equilibrium contact time 1 h. It has been found that the adsorption process mainly follows pseudo-second-order kinetics and intraparticle diffusion model. The adsorption isotherms were better adjusted by the Langmuir–Freundlich model ($R^2 > 0.96$). Thermodynamic parameters indicate that the adsorption process of BB41 is spontaneous, endothermic physics in nature for the both materials.

References

- [1] M. Iqbal, M. Abbas, A. Nazir, Bioassays based on higher plants as excellent dosimeters for ecotoxicity monitoring: a review, *Chem. Int.*, 5 (2019) 1–80.
- [2] H.X. Wang, G.Z. Li, A. Fakhri, Fabrication and structural of the Ag₂S-MgO/graphene oxide nanocomposites with high photocatalysis and antimicrobial activities, *J. Photochem. Photobiol., B*, 207 (2020) 111882, <https://doi.org/10.1016/j.jphotobiol.2020.111882>.
- [3] G.L. Wang, A. Fakhri, Preparation of CuS/polyvinyl alcohol-chitosan nanocomposites with photocatalysis activity and antibacterial behavior against G⁺/G⁻ bacteria, *Int. J. Biol. Macromol.*, 155 (2020) 36–41.
- [4] M. Iqbal, *Vicia faba* bioassay for environmental toxicity monitoring: a review, *Chemosphere*, 144 (2016) 785–802.
- [5] M. Lu, Y.X. Cui, S.X. Zhao, A. Fakhri, Cr₂O₃/cellulose hybrid nanocomposites with unique properties: facile synthesis, photocatalytic, bactericidal and antioxidant application, *J. Photochem. Photobiol., B*, 205 (2020) 111842, <https://doi.org/10.1016/j.jphotobiol.2020.111842>.
- [6] A.M.K. Pasha, M. Hosseini, A. Fakhri, V.K. Gupta, S. Agarwa, Investigation of photocatalytic process for iron disulfide-bismuth oxide nanocomposites by using response surface methodology: structural and antibacterial properties, *J. Mol. Liq.*, 289 (2019) 110950, <https://doi.org/10.1016/j.molliq.2019.110950>.
- [7] A. Fakhri, V.K. Gupta, H. Rabizadeh, S. Agarwal, N. Sadeghi, S. Tahami, Preparation and characterization of WS₂ decorated and immobilized on chitosan and polycaprolactone as

- biodegradable polymers nanofibers: photocatalysis study and antibiotic-conjugated for antibacterial evaluation, *Int. J. Biol. Macromol.*, 120 (2018) 1789–1793.
- [8] H. Pan, H.X. Xie, G. Chen, N.B. Xu, M.M. Wang, A. Fakhri, Cr₂S₃-Co₂O₄ on polyethylene glycol-chitosan nanocomposites with enhanced ultraviolet light photocatalysis activity, antibacterial and antioxidant studies, *Int. J. Biol. Macromol.*, 148 (2020) 608–614.
- [9] M. Ahmaruzzaman, A review on the utilization of fly ash, *Prog. Energy Combust. Sci.*, 36 (2010) 327–363.
- [10] H. Katsumata, Y. Oda, S. Kaneco, T. Suzuki, Photocatalytic activity of Ag/CuO/WO₃ under visible-light irradiation, *RSC Adv.*, 3 (2013) 5028–5035.
- [11] X.J. Li, Z.J. Zhang, A. Fakhri, V.K. Gupta, S. Agarwal, Adsorption and photocatalysis assisted optimization for drug removal by chitosan-glyoxal/polyvinylpyrrolidone/MoS₂ nanocomposites, *Int. J. Biol. Macromol.*, 136 (2019) 469–475.
- [12] N. Mahrez, S. Bendenia, K. Marouf-Khelifa, I. Batonneau-Gener, A. Khelifa, Improving of the adsorption capacity of halloysite nanotubes intercalated with dimethyl sulfoxide, *Compos. Interfaces*, 22 (2015) 403–417.
- [13] J. Fu, Y.-J. Chen, J.-Y. Ju, Q.-S. Li, S.-Q. An, H.-L. Zhu, Treating dye wastewater of reactive brilliant red K-2BP by cetyltrimethylammonium chloride-modified bentonite with polyacrylamide flocculant, *Pol. J. Stud. Environ.*, 20 (2011) 61–66.
- [14] D.L. Guerra, C. Airoidi, Anchored thiol smectite clay—kinetic and thermodynamic studies of divalent copper and cobalt adsorption, *J. Solid State Chem.*, 181 (2008) 2507–2515.
- [15] A.M. Awwad, M.W. Amer, M.M. Al-Aqarbeh, TiO₂-kaolinite nanocomposite prepared from the Jordanian Kaolin clay: adsorption and thermodynamics of Pb(II) and Cd(II) ions in aqueous solution, *Chem. Int.*, 6 (2020) 168–178.
- [16] E.C. Jennifer, O.P. Ifedi, Modification of natural bentonite clay using cetyl trimethyl-ammonium bromide and its adsorption capability of some petrochemical wastes, *Chem. Int.*, 5 (2019) 269–273.
- [17] J. da Silva Favero, V. dos Santos, V. Weiss-Angeli, L.B. Gomes, D.G. Veras, N. Dani, A.S. Mexias, C.P. Bergmann, Evaluation and characterization of Melo Bentonite clay for cosmetic applications, *Appl. Clay Sci.*, 175 (2019) 40–46.
- [18] D. Kurnosov, A. Burakov, I. Burakova, Development of a bentonite clay/carbon nanotubes composite for liquid-phase adsorption, *Mater. Today Proc.*, 11 (2019) 398–403.
- [19] F. Bergaya, B.K.G. Theng, G. Lagaly, Chapter 7 – Modified Clays and Clay Minerals, F. Bergaya, B.K.G. Theng, G. Lagaly, Eds., *Handbook of Clay Science*, Elsevier, Amsterdam, 2006, pp. 393–422.
- [20] R.B. Valapa, S. Loganathan, G. Pugazhenth, S. Thomas, T.O. Varghese, Chapter 2 – An Overview of Polymer-Clay Nanocomposites, K. Jlassi, M.M. Chehimi, S. Thomas, Eds., *Clay-Polymer Nanocomposites*, Elsevier, Amsterdam, The Netherlands, 2017, pp. 29–81.
- [21] L. Nikolic, I. Ristic, S. Stojiljkovic, Z. Vukovic, D. Stojiljkovic, V. Nikolic, J. Budinski-Simendic, The influence of montmorillonite modification on the properties of composite material based on poly(methacrylic acid), *J. Compos. Mater.*, 46 (2011) 921–928.
- [22] N. Ozturk, A. Tabak, S. Akgol, A. Denizli, Newly synthesized montmorillonite-histidine (Bent-Hist) microcomposite affinity sorbents for IgG adsorption, *Colloids Surf., A*, 301 (2007) 490.
- [23] C.H. Zhou, D.S. Tong, W.H. Yu, Chapter 7 – Smectite Nanomaterials: Preparation, Properties, and Functional Applications, A.Q. Wang, W.B. Wang, Eds., *Nanomaterials from Clay Minerals A New Approach to Green Functional Materials: A Volume in Micro and Nano Technologies*, Elsevier, Amsterdam, The Netherlands, 2019, pp. 335–364.
- [24] M. Huskić, A. Anžlovar, M. Žigon, Montmorillonite-phenolic resin nanocomposites prepared by one-step in-situ intercalative polymerisation, *Appl. Clay Sci.*, 101 (2014) 484–489.
- [25] A. Berrazoum, R. Marouf, F. Ouadjenia, J. Schott, Bioadsorption of a reactive dye from aqueous solution by municipal solid waste, *Biotechnol. Rep. (Amst)*, 7 (2015) 44–50.
- [26] S. Lagergren, Zur theorie der sogenannten adsorption gelosterstoffe (About the theory of so-called adsorption of soluble substances), *Kungliga Svenska Vetenskapsademiens Handlingar (K. Sven. Vetenskapsakad. Handl.)*, 24 (1898) 1–39.
- [27] Y.S. Ho, G. McKay, Pseudo-second-order model for sorption processes, *Process Biochem.*, 34 (1999) 451–465.
- [28] W.J. Weber, J.C. Morris, Kinetics of adsorption on carbon from solution, *J. Sanitary Eng. Div.*, 89 (1963) 31–59.
- [29] I. Langmuir, The adsorption of gases on plane surfaces of glass, mica and platinum, *J. Am. Chem. Soc.*, 40 (1918) 1361–1403.
- [30] H.M.F. Freundlich, Over the adsorption in solution, *J. Phys. Chem.*, 57 (1906) 385–470.
- [31] O. Hamdaoui, E. Naffrechoux, Modeling of adsorption isotherms of phenol and chlorophenols onto granular activated carbon: Part II. Models with more than two parameters, *J. Hazard. Mater.*, 147 (2007) 401–411.
- [32] F. Zahaf, N. Dali, R. Marouf, F. Ouadjenia, J. Schott, Application of hydroxy-aluminum- and cetyltrimethylammonium bromide-intercalated bentonite for removing acid and reactive dyes, *Desal. Water Treat.*, 57 (2015) 21045–21053.
- [33] N. Boudouara, N. Dali, R. Marouf, F. Ouadjenia, J. Schott, Removal of Chlorothalonil from water by a bentonite treated chemically, *J. Mater. Environ. Sci.*, 12 (2017) 4523–4531.
- [34] A. Usuki, Y. Kojima, M. Kawasumi, A. Okada, Y. Fukushima, T. Kurauchi, O. Kamigaito, Synthesis of nylon 6-clay hybrid, *J. Mater. Res.*, 8 (1993) 1179–1184.
- [35] P.B. Messersmith, E.P. Giannelis, Synthesis and characterization of layered silicate-epoxy nanocomposites, *Chem. Mater.*, 6 (1994) 1719–1725.
- [36] R.L. Frost, J. Kristof, E. Horvath, J.T. Klopogge, Rehydration and phase changes of potassium acetate-intercalated halloysite at 298 K, *J. Colloid Interface Sci.*, 226 (2000) 318–327.
- [37] R.L. Frost, J. Kristof, G.N. Paroz, J.T. Klopogge, Role of water in the intercalation of kaolinite with hydrazine, *J. Colloid Interface Sci.*, 208 (1998) 216–225.
- [38] M.J. Wilson, *Clay Mineralogy: Spectroscopic and Chemical Determinative Methods*, Chapman & Hall, London, 1995.
- [39] I. Poljanšek, M. Krajnc, Characterization of phenol-formaldehyde prepolymer resins by in line FT-IR Spectroscopy, *Acta Chim. Slov.*, 52 (2005) 238–244.
- [40] I. Humelnicu, A. Băiceanu, M.-E. Ignat, V. Dulman, The removal of Basic Blue 41 textile dye from aqueous solution by adsorption onto natural zeolitic tuff: kinetics and thermodynamics, *Process Saf. Environ. Prot.*, 105 (2017) 274–287.
- [41] C.G. Chen, T.B. Tolle, Fully exfoliated layered silicate epoxy nanocomposites, *J. Polym. Sci., Part B: Polym. Phys.*, 42 (2004) 3981–3986.
- [42] I.D. Mall, V.C. Srivastava, N.K. Agarwal, I.M. Mishra, Adsorptive removal of malachite green dye from aqueous solution by bagasse fly ash and activated carbon-kinetic study and equilibrium isotherm analyses, *Colloids Surf., A*, 264 (2005) 17–28.
- [43] S. Kadi, S. Lellou, K. Marouf-Khelifa, J. Schott, A. Khelifa, Cadmium(II) and lead(II) removal from aqueous solutions by heat-treated Algerian halloysite, *Desal. Water Treat.*, 113 (2018) 213–226.
- [44] Z. Rawajfeh, N. Nsour, Thermodynamic analysis of sorption isotherms of chromium(VI) anionic species on reed biomass, *J. Chem. Thermodyn.*, 40 (2008) 846–851.
- [45] F.A. Batzias, D.K. Sidiras, Simulation of methylene blue adsorption by salts-treated beech sawdust in batch and fixed-bed systems, *J. Hazard. Mater.*, 149 (2007) 8–17.
- [46] K.G. Bhattacharyya, S.S. Gupta, Adsorption of Fe(III), Co(II) and Ni(II) on ZrO-kaolinite and ZrO- montmorillonite surfaces in aqueous medium, *Colloids Surf., A*, 317 (2008) 71–79.
- [47] A.A. Adeyemo, I.O. Adeoye, O.S. Bello, Adsorption of dyes using different types of clay: a review, *Appl. Water Sci.*, 7 (2017) 543–568.
- [48] A. Kausar, K. Naeem, T. Hussain, Zill-i-Huma Nazli, H.N. Bhatti, F. Jubeen, A. Nazir, M. Iqbal, Preparation and characterization of chitosan/clay composite for direct Rose FRN dye removal from aqueous media: comparison of linear and non-linear regression methods, *J. Mater. Res. Technol.*, 8 (2019) 1161–1174.

- [49] S. Lellou, S. Kadi, L. Guemou, J. Schott, H. Benhebal, Study of methylene blue adsorption by modified kaolinite by dimethyl sulfoxide, *Ecol. Chem. Eng. S*, 27 (2020) 225–239.
- [50] B.K. Nandi, A. Goswami, M.K. Purkait, Adsorption characteristics of brilliant green dye on kaolin, *J. Hazard. Mater.*, 161 (2009) 387–395.
- [51] M. Yazdanshenas, K. Farizadeh, A. Fazilat, S. Ahmadi, Adsorption of Basic Blue 41 from aqueous solution onto coconut fiber particles, *J. Appl. Chem. Res.*, 2 (2014) 15–28.
- [52] M. Zarezadeh-Mehrizi, A. Badii, Highly efficient removal of Basic Blue 41 with nanoporous silica, *Water Sci. Ind.*, 5 (2014) 49–57.
- [53] C.H. Giles, T.H. MacEwan, S.N. Nakhwa, D. Smith, Studies in adsorption. Part XI. A system of classification of solution adsorption isotherms, and its use in diagnosis of adsorption mechanisms and in measurement of specific surface areas of solids, *J. Chem. Soc.*, 973 (1960) 3973–3993.
- [54] M.A. Hossain, M. Mohibullah, Kinetics and thermodynamics of adsorption of Basic Blue 41 on used black tea leaves, *Int. J. Sci. Eng. Res.*, 8 (2017) 995–1002.
- [55] N.Sh. El-Gendy, R.A. El-Salamony, S.S. Abu Amr, H.N. Nassar, Statistical optimization of Basic Blue 41 dye biosorption by *Saccharomyces cerevisiae* spent waste biomass and photo-catalytic regeneration using acid TiO_2 hydrosol, *J. Water Process Eng.*, 6 (2015) 193–202.
- [56] A.M. Aljeboree, A.N. Alshirifi, A.F. Alkaim, Kinetics and equilibrium study for the adsorption of textile dyes on coconut shell activated carbon, *Arabian J. Chem.*, 10 (2017) S3381–S3393.
- [57] F. Kooli, Y. Liu, R. Al-Faze, A. Al Suhaimi, Effect of acid activation of Saudi local clay mineral on removal properties of Basic Blue 41 from an aqueous solution, *Appl. Clay Sci.*, 116–117 (2015) 23–30.
- [58] S. Afshin, S.A. Mokhtari, M. Vosoughi, H. Sadeghi, Y. Rashtbari, Data of adsorption of Basic Blue 41 dye from aqueous solutions by activated carbon prepared from filamentous algae, *Data Brief*, 21 (2018) 1008–1013.
- [59] Y.H. Jiang, Y.Y. Luo, F.M. Zhang, L.Q. Guo, L. Ni, Equilibrium and kinetic studies of C.I. Basic Blue 41 adsorption onto N, F-codoped flower-like TiO_2 microspheres, *Appl. Surf. Sci.*, 273 (2013) 448–456.
- [60] M.J. Jaycock, G.D. Parfitt, *Chemistry of Interfaces*, Ellis Horwood Ltd., Onichester, 1981, p. 625.
- [61] S.S. Gupta, K.G. Bhattacharyya, Immobilization of Pb(II), Cd(II) and Ni(II) ions on kaolinite and montmorillonite surfaces from aqueous medium, *J. Environ. Manage.*, 87 (2008) 46–58.